Iterative Synthesis of Contorted Macromolecular Ladders for Fast-Charging and Long-Life Lithium Batteries

Zexin Jin[1]*†, Qian Cheng[1]†, Si Tong Bao[1], Ruiwen Zhang[2], Austin M. Evans[1], Fay Ng[1], Yunyao Xu[1], Michael L. Steigerwald[1], Ann E. McDermott[1], Yuan Yang[2]*, Colin Nuckolls[1]*

[1]Department of Chemistry, Columbia University, New York, New York 10027, United States

[2]Department of Applied Physics and Applied Mathematics, Columbia University, New York, New York 10027, United States

ABSTRACT: We report here an iterative synthesis of long helical perylene diimide (**hPDI[n]**) nanoribbons with the length up to 16 fused benzene rings. These contorted, ladder-type conjugated, and atomically precise nanoribbons show great potential as organic fast-charging and long-lifetime battery cathodes. By tuning the length of the **hPDI[n]** oligomers, we can simultaneously modulate the electrical conductivity and ionic diffusivity of the material. The length of the ladders adjusts both the conjugation for electron transport and the contortion for lithium-ion transport. The longest oligomer, **hPDI[6]**, when fabricated as the cathode in lithium batteries, features both high electrical conductivity and high ionic diffusivity. This electrode material exhibits a high power density and can be charged in less than one minute to 66% of its maximum capacity. Remarkably, this material also has exceptional cycling stability and can operate 10,000 charging-discharging cycles without any appreciable capacity decay. The design principles described here chart a clear path for organic battery electrodes that are sustainable, fast-charging, and long lasting.

INTRODUCTION

Lithium-ion batteries (LIBs)[1–3] are the world's predominant energy storage devices and as such have significantly accelerated the development of today's digital information society.[4–6] While current LIBs boast amazing performance, their power density and cycling stability are areas in need of improvement.[7–12] This need is particularly acute for many applications, such as electric vehicles, due to the relatively long charging time and cycling capacity loss associated with current battery technologies.[13] Compared to the current inorganic electrode materials, organic electrode materials (OEMs) provide unique opportunities to achieve high power density through molecular engineering that can, in principle, yield simultaneously high ionic diffusivity and high specific capacities.[14–19] Further, OEMs benefit from being sustainable and "green" due to the earth abundance of their components, low cost to produce, and low environmental impact.[20–22] However, one of the major issues regarding OEMs is their trade-off between specific capacity and cycling stability.[18] Organic molecules, albeit with high capacity, leach into the electrolyte solution during the redox reactions, which results in poor cycling stability. Organic polymers can overcome the dissolution issue, but they typically have low charge capacity due to the redox-inactive nature of their linkers and solubilizing side chains. Beyond these challenges, the low intrinsic electrical conductivity of OEMs has thwarted their ability to achieve high rate capability and high areal mass-loading.[17] Consequently, incorporating a high ratio of conductive additives is usually necessary in electrode fabrication for organics to achieve idealized results, which further limits OEMs' technological utility.[17,19]

Here we describe a molecular design of contorted, fully-conjugated, atomically precise, electroactive molecular ladders that simultaneously solves the fundamental issues associated with the existing classes of OEMs. These conjugated molecular ladders shown in Figure 1a, known as the helical perylene diimide (**hPDI[n]**), are significant because they have proven useful in photovoltaics,[23] photosensors,[24] field effect transistors,[25] pseudocapacitors,[26] and as the electron transport layer in perovskite solar cells.[27] Despite their good performance and excellent characteristics, the synthesis of the **hPDI[n]** series is not effective to synthesize ribbons that are longer than four PDI subunits (i.e., **hPDI[4]**).[25] This manuscript describes a new synthetic method that allows them to be synthesized in longer form with up to 16 fused benzene rings (**hPDI[6]**, Figure 1b), allowing us to study the optoelectronic properties of the family. Furthermore, we demonstrated these molecular ladders have great potential as fast-charging and long-life OEMs. The most efficacious member of this series, **hPDI[6]**, highlights four design principles for organic electrodes to achieve exceptional rate capability and cycling stability (Figure 1b): (1) redox-active PDI subunits that feature high stability and fast redox kinetics;[28,29] (2) insoluble macromolecules that overcome the dissolution issue associated with small molecules; (3) molecular contortion that facilitates lithium-ion transport and thus leads to high ionic diffusivity within the solid material;[30] (4) precisely defined fully conjugated ladder structure that provides high electrical conductivity.

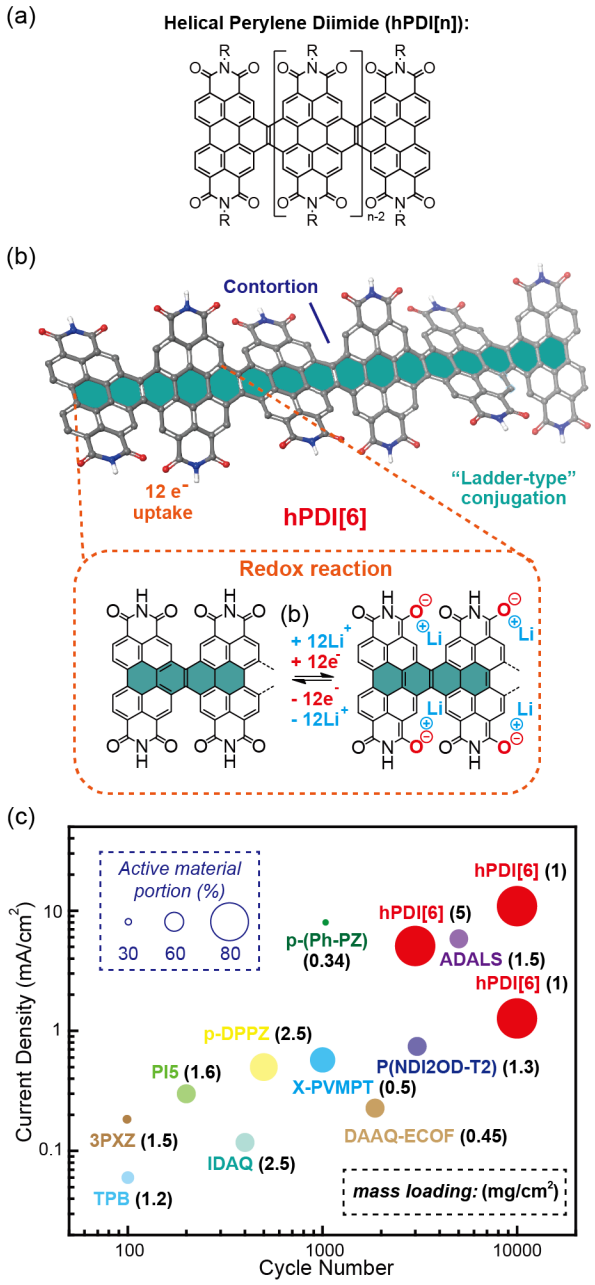

Figure 1. (a) Helical perylene diimide nanoribbons. (b) The schematics of **hPDI[6]** as fast charging lithium battery cathode. (c) Performance comparison of **hPDI[6]** with other reported OEMs with similar mass loadings and specific capacities (100-250 mAh/g). The active material portions are indicated by the size of the circles, the average active material mass loadings are shown in parentheses. The three red circles for **hPDI[6]** represent three different cells cycled at different current or mass loading. See Table S1 (Supporting Information) for detailed information used in this graph.

When **hPDI[6]** is formulated as a cathode, it shows excellent rate performance of 126 mAh/g and 87 mAh/g (96% and 66% retention of their theoretical capacity) under a current density of 1 A/g (7.7 C) and 10 A/g (77 C), respectively. Such high rate performance significantly reduces the charging time to less than one minute, and leads to an output power density up to 22,500 W/kg. Moreover, **hPDI[6]** cathodes exhibit exceptional cycling stability over 10,000 charge-discharge cycles with capacity fade of 0.004% and 0.0017% per cycle for 7.7 C and 77 C, respectively. Importantly, these **hPDI[6]** cathodes are fabricated with a high active material portion of 80 wt.%, which is unusually high for organic electrodes.[19] Figure 1c displays the particular advantages of this design over state-of-art organic cathodes by its rate performance, cycling stability and active material portion. To demonstrate the practical relevance, we assembled coin cells with high active mass loading (5 mg/cm^2, shown in Figure 1c) and with high temperature (60 °C) operation capability, and pouch cells that are able to power a commercial LED fan. This new material and the associated design strategy set forth a path for sustainable, fast-charging and long lifetime organic batteries.

RESULTS AND DISCUSSION

Iterative Synthesis of hPDI[n]. PDI-based molecules and polymers have been investigated as electrode materials by other research groups because of its stable redox reaction. However, due to densely packed structure and low electrical conductivity,[31] the materials showed limited power density and poor cycling stability (Table S2). We hypothesized that the electrical conductivity and ionic diffusion could be simultaneously improved by increasing both the length of π-conjugation and the number of contorted aromatic sites. In addition, a longer fully conjugated system can stabilize the reduced states thus make the redox-active groups more accessible (Figure 1b). Critical to this study was the need to synthesize atomically defined, ladder-type fully conjugated structures of substantial length. However, previous synthetic approaches[32] used to synthesize **hPDI[n]** (up to n = 4) does not allow the production of longer ribbons due to incomplete photocyclization.

Two observations guided our synthetic plan for the preparation of the longer oligomers. First, in our prior synthesis of **hPDI[4]**, we found that the photo cyclization of the precursor with an internal double bond flanked by two **hPDI[2]** precursors results in recovery of the starting material and essentially no photocyclization.[25] Second, previous reports[33] indicate that the photocyclization on PDI to form benzo-PDI (formation of the A-bond in Figure 2a) is much more facile than the photocyclization to the coronenediimide (formation of the B-bond in Figure 2a). Putting these two factors together, we hypothesized that the formation of "Type B" precursors in Figure 2b would lead to an efficient and high yielding synthesis of **hPDI[5]-C11** and **hPDI[6]-C11** (C11 refers to the branched undecyl solubilizing groups).

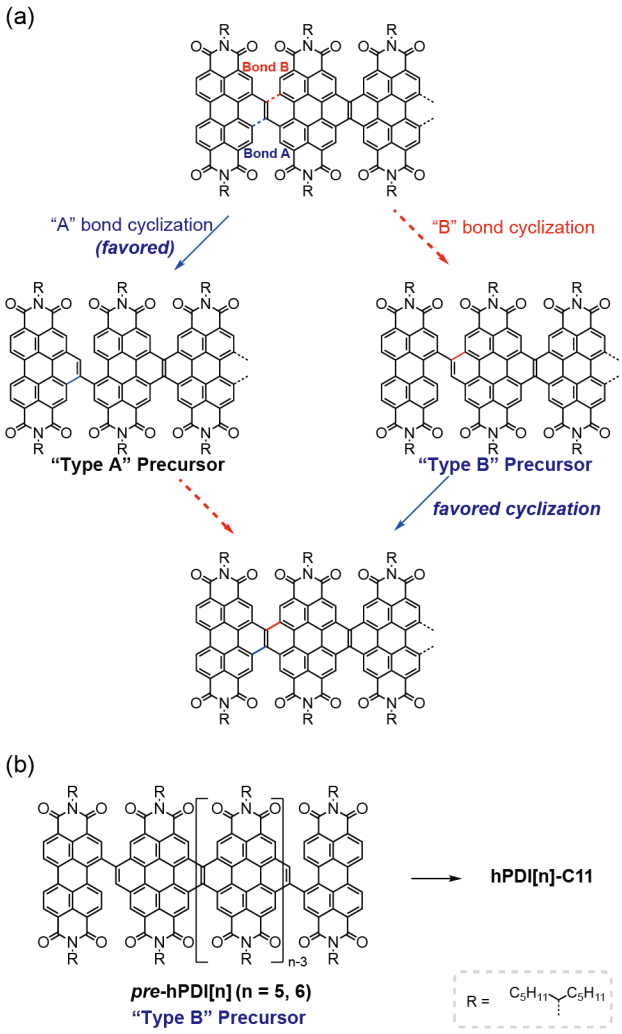

Figure 2. (a) Cyclization sequence of **hPDI[n]** precursors. (b) Hypothesized precursors for longer **hPDI[n]** ribbons.

Scheme 1 displays the iterative synthesis of **hPDI[5]-C11** and **hPDI[6]-C11** from shorter ribbons **hPDI[3]-C11** and **hPDI[4]-C11**, respectively. We first dibrominated **hPDI[3]-C11** using large excess of bromine in dichloromethane at room temperature. Since MIDA boronates can serve as masked boronic acid reagent,[34–36] we installed ethylene N-methyliminodiacetate (MIDA) boronate group on **hPDI[3]** by Suzuki coupling of with *trans*-2-(pinacol boronate)vinylboronic acid MIDA ester. We then subject the **DiBmida-hPDI[3]** to Mallory photocyclization using iodine and light under room temperature. We deprotect the MIDA boronates and react this with PDI-Br to give "Type B" precursor ***pre*-hPDI[5]**. To complete the synthesis of **hPDI[5]-C11**, we irradiate ***pre*-hPDI[5]** with a common visible light LED in the presence of iodine in chlorobenzene at 90 °C. **hPDI[5]** formed quantitively in two hours. We purify the product by simply removing the solvent and washing with methanol. Using this same approach, we synthesized **hPDI[6]-C11** from **hPDI[4]-C11**. Importantly, this new procedure is applicable to longer and functionalized **hPDI[n]** nanoribbons. We then performed vacuum thermolysis on **hPDI[n]-C11** at 360 °C to quantitatively remove the alkyl chains (see thermogravimetric analysis, Figure S1). The resulting **hPDI[n]** exhibit enhanced gravimetrical capacity by reducing the electro-inactive mass and simultaneously renders the material insoluble (Figure S28). **hPDI[2]** was not included due to the unsuccessful thermolysis from corresponding **hPDI[2]-C11**. The structure of **hPDI[n]** (n=3–6) was confirmed by ^{13}C solid-state NMR, infrared spectroscopy and MALDI mass spectrometry (characterization and synthetic details can be found in Supporting Information, section 2&3).

Scheme 1. Synthesis of **hPDI[5]-C11**, **hPDI6-C11** and **hPDI[n]** (n=3–6).

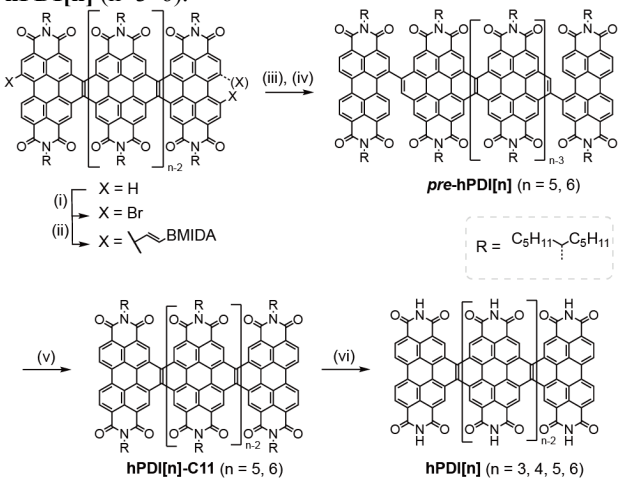

Reaction conditions: (i) Br_2, CH_2Cl_2, rt. (ii) *trans*-2-(pinacol boronate)vinylboronic acid MIDA ester, $Pd(dppf)Cl_2$, K_3PO_4, THF/H_2O, rt. (iii) I_2, DCM, hν, rt. (iv) PDI-Br, $Pd(dppf)Cl_2$, K_2CO_3, THF/H_2O, 57 °C. (v) I_2, PhCl, hν, 90 °C. (vi) 360 °C, in the vacuum. MIDA: N-Methyliminodiacetate.

Electrical conductivity and effective conjugation length of hPDI[n].

We measured the electrical conductivity of the **hPDI[n]** (n = 3–6) thin films by a two-probe method (Figure 3b and Figure S4). The electrical conductivity of **hPDI[5]** and **hPDI[6]** are one order of magnitude higher than those of shorter ribbons. Such high conductivity is attributed to both the extended ladder conjugation and the array of hydrogen bond donors and acceptors on the primary imide organizing the nanowires.[37] The important conclusion is that the electrical conductivity of the **hPDI[n]** family increases as the ribbons are extended. We estimated the HOMO-LUMO gap of hPDI[n] ribbons from electronic absorption maxima of their alkylated counterpart, **hPDI[n]-C11**. We used Meier's method[38] to determine the bandgap of infinite **hPDI[n]** polymers to be 1.96 eV, which suggests that **hPDI[6]** (with a bandgap of 2.00 eV) is a good proxy for the polymeric **hPDI[n]** structures (Figure S2). Therefore, the improvement of electrical conductivity originates from the lengthy conjugated structure of hPDI[n]. To note, these conductivities are from the undoped molecules, and their anionic forms after reduction presumably have much higher conductivities.[39] Taken together, these results show that increasing the length of the conjugated ribbons is an effective way to improve the electrical conductivity.

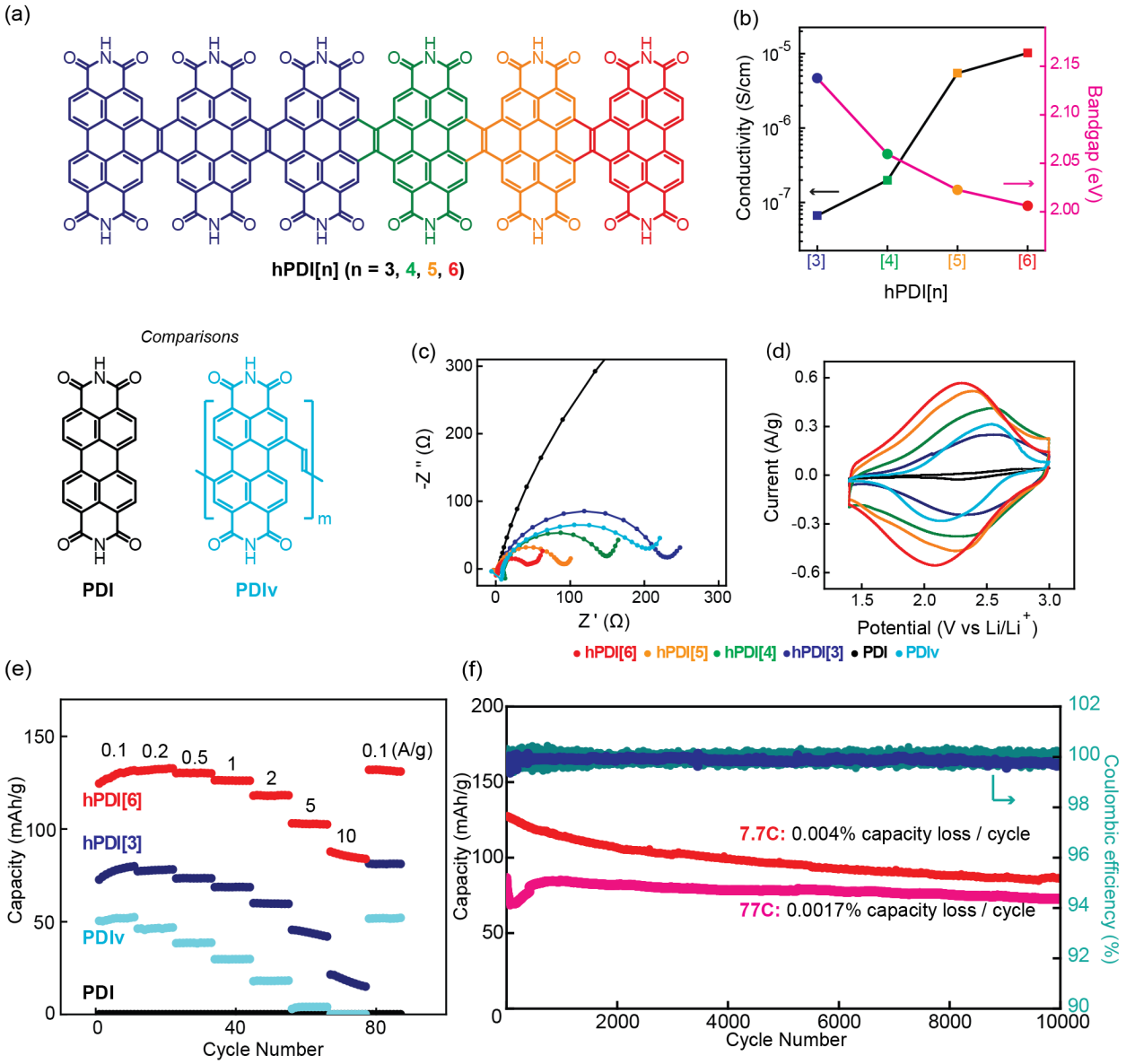

Figure 3. The electrochemical characterization of hPDI[n]. (a) Molecular structures of the compounds for comparative studies: **hPDI[3]** (blue), **hPDI[4]** (green), **hPDI[5]** (orange), **hPDI[6]** (red), **PDI** (black) and **PDIv** (cyan). (b) Electrical conductivities and bandgaps of **hPDI[n]**. Bandgaps were estimated from the optical energy gaps of **hPDI[n]-C11**s. (c) EIS and (d) CV (scan rate: 1 mV/s) of all cathode materials. (e) Rate performance of **PDI**, **PDIv**, **hPDI[3]** and **hPDI[6]**. (f) Cycling performance of **hPDI[6]** at 7.7C (1 A/g, capacity in red and Coulombic efficiency in cyan) and 77C (10 A/g, capacity in pink and Coulombic efficiency in blue.

Electrochemical performance of hPDI[n]. To evaluate the electrochemical performance of **hPDI[n]**, we prepared the electrodes by drop casting a slurry of 80 wt.% **hPDI[n]**, 10 wt.% carbon black (as conductive agent) and 10 wt.% polyvinylidene fluoride (PVDF, as binder) in N-methyl-2-pyrrolidone onto a carbon paper. The carbon paper, which is a common current collector just like nickel foam, is used here because of their ability to hold the diluted slurries. Such high portion of active material is typical for tests of inorganic materials but is much higher than those typically tested in organic materials.[19] The electrodes were then assembled with lithium metal and 1 M $LiPF_6$ in ethylene carbonate (EC)/diethyl carbonate (DEC) (1:1 by volume) electrolyte in 2032 coin cells. For comparison, we also investigated the **PDI** monomer and a PDI-vinyl conjugated polymer (**PDIv**, section 2.3 of Supporting Information provides synthetic details) with similar theoretical gravimetric capacities (Figure 3a). The electrochemical impedance spectroscopy (EIS) of these cells reveals that the charge-transfer resistance (R_{ct}) for **hPDI[n]** decreases as the ribbon is made longer (Figure 3c), PDI exhibits a high R_{ct} of 1400 Ω (Table S3) and **PDIv** exhibits similar R_{ct} as **hPDI[3]**. This trend of R_{ct} correlates well with the electrical conductivity of the pristine materials (Table S3). The low charge transfer resistance of **hPDI[6]** (47 Ω) facilitates fast electron transport, presumably resulting from fast intramolecular and intermolecular charge transfer.

We next performed cyclic voltammograms (CV) to examine the electrochemical behaviors of **hPDI[n]** (n = 3–6), **PDI** and **PDIv** (Figure 3d and Figure S29). At a scan rate of 1 mV/s, **hPDI[n]** displayed a broad and reversible redox couple at a potential of 2.25 V vs Li/Li^+, matching the redox events of PDI subunits. The peak current of **hPDI[n]** increases as the ribbon

length increases, revealing the improved electrochemical performance as [n] increases. Analysis on the log-log plot of the sweep rate (v) versus the peak current (i) shows that **hPDI[n]** ribbons exhibited surface-controlled kinetics, **PDI** exhibited diffusion-controlled behavior, and **PDIv** was in-between (Figure S30). To further demonstrate the contortions effect on lithium-ion transport, we investigate the lithium-ion diffusivity (D_{Li+}) obtained by EIS (Figure S31 and Table S3).[40,41] For **hPDI[n]** series, the D_{Li+} increases as the length of the macromolecule increases from **hPDI[3]** (1.8×10^{-11} cm^2/s) to **hPDI[6]** (5.7×10^{-10} cm^2/s, Table S3). This D_{Li+} increment as the ribbons extended longer is attributed to both the increase in particle surface area (Figure S6) and the more well-defined contorted carbonyl position. The **PDIv** conjugated polymer, however, exhibited a significantly lower diffusion coefficient of 1.9×10^{-11} cm^2/s. Such lower diffusivity of **PDIv** indicates the importance of well-defined position of the carbonyls imposed by molecular contortion in the longer oligomers.

With significantly improved electrical conductivity and ionic diffusivity, **hPDI[6]** achieves exceptional power density and best-in-class cycling stability as a cathode material. Figure 3e displays the increasing rate capability from **PDI**, **PDIv** and **hPDI[3]** to **hPDI[6]** at different discharge rates (the rate performance of **hPDI[4]** and **hPDI[5]** can be found in Figure S32). Multiple tests were performed to confirm that the PDI monomer has a minuscule capacity at 80% active material mass loading. At 0.1 A/g (0.77 C), **hPDI[6]** has reached 99% of the theoretical specific capacity value (131 mAh/g). It is important to note that **hPDI[6]** exhibits almost no loss in capacity until the rate of the current was increased to 2 A/g. Even at a 100-fold current rate of 10 A/g (77 C), **hPDI[6]** boasted a specific capacity of 87 mAh/g. These results suggest that **hPDI[6]** batteries are able to be charged to 66% of its capacity within 35 seconds, corresponding to a specific power density of 22,500 W/kg. We attribute this exceptional rate performance of **hPDI[6]** to both high ionic diffusivity from the molecular contortion and high electrical conductivity from the precisely defined, "ladder-type" conjugated structure. Recently, Abruña, Fors and coworkers[42] reports an elegant work on phenazine-based OEMs with high energy and power densities by cross-linking, which also demonstrates the effect of increasing conjugation. Importantly, **hPDI[6]** cathode exhibits extraordinary cycling stability (Figure 3f). At 1 A/g, **hPDI[6]** has an initial capacity of 126 mAh/g and preserves 86 mAh/g after 10,000 cycles at 7.7 C, corresponding to capacity fade of only 0.004% each cycle. At a higher rate (10 A/g, 77 C), **hPDI[6]** cathode also maintains its stability, with 84% capacity retention over 10,000 cycles, corresponding to an ultra-low capacity 0.0017% loss per cycle. To note, all the **hPDI[n]** (n = 3–6) cathodes exhibited extraordinary cycling stability (Figure S33). There is a large overpotential from lithium metal which may result in electrochemical irreversibility and capacity loss when the batteries are operated at high current density. Even so, these batteries can cycle for 10,000 cycles with no issue. Collectively, the **hPDI[6]** is a very promising fast-charging cathode for its high power density and cycling stability to fill the absence between supercapacitor and batteries.

High mass loading and high temperature test of hPDI[6]. Besides the high rate performance and cycling lifetime, **hPDI[6]** cathodes are able to maintain their superior performance in both high mass loading and high temperature conditions. To date, most research using organic materials as electrodes are limited to a low mass loading around 0.1~1 mg/cm^2 due to materials' low intrinsic electrical conductivity.[14] To investigate the high active mass loading ability of **hPDI[6]**, we fabricated the electrodes with an active material loading of 5 mg/cm^2. This material loading is not only a practical mass loading but amongst the highest ever reported in an organic cathode material (Table S1). As shown in Figure 4a, these cells with high active mass loading were able to maintain 92% of the theoretical specific capacity (121 mAh/g) at 1 A/g, and still exhibit high cycling stability with 75% capacity retention after 3,000 cycles. Furthermore, **hPDI[6]** cathodes also exhibit reliable high temperature performance with an initial capacity of 131 mAh/g and 71% capacity retention after 1000 cycles at 60 °C (Figure 4b).

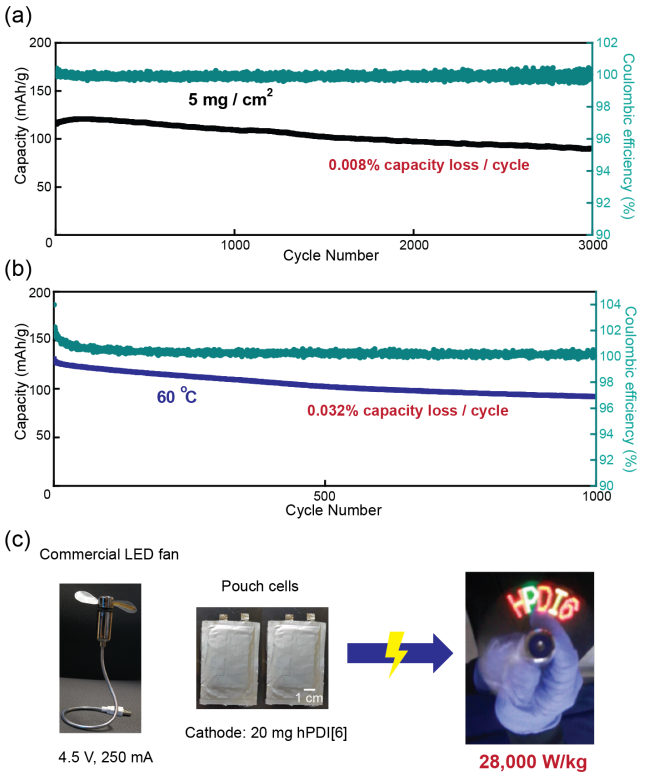

Figure 4. Demonstration of practical application of **hPDI[6]** batteries. (a) The high mass loading of **hPDI[6]** batteries with an areal mass loading of 5 mg/cm^2. (b) The 60 °C high temperature test. The mass loading is 1 mg/cm^2. (c) The scheme of **hPDI[6]** batteries powering a LED fan.

Practical demonstration of hPDI[6]. Finally, we demonstrated the practical relevance of **hPDI[6]** materials by fabricating pouch cells to power a commercial LED fan. The working voltage and current of the fan are 4-5 V and 200-300 mA, respectively, corresponding to a total power of ~1.12 W. Accordingly, we built pouch cells with an electrode area of 20 cm^2 and a cathode composite containing 20 mg of **hPDI[6]**. Two pouch cells were connected in series to provide enough voltage. As shown in Figure 4c and the Supplemental Video, the battery was able to power the LED fan for 30 seconds, corresponding to a power density of 28,000 W/kg. Such power density is 50-fold beyond current state-of-the-art LIBs. These results show that **hPDI[6]** can be easily integrated into existing battery manufacturing processes.

CONCLUSION

In summary, we designed and introduced a contorted, atomically defined **hPDI[6]** macromolecular ladder with high ionic diffusivity and electrical conductivity as a fast-charging and long-lifetime battery cathode. **hPDI[n]** was efficiently synthesized via a newly developed iterative protocol. We found that the electrical conductivity of **hPDI[n]** can be engineered and significantly improved by increasing the conjugation length of the ribbons. In addition, longer **hPDI[n]** ribbons also introduce more contortion sites to accelerate the ion transport. With improved electrical conductivity and ion diffusivity, **hPDI[6]** cathodes show a power density two orders of magnitude higher than the conventional inorganic materials. Batteries with **hPDI[6]** as a cathode can be charged to 66% of its maximum capacity within 35 seconds. Meanwhile, the stable structure of **hPDI[6]** allows it to cycle 10,000 times without significant capacity decay. Moreover, **hPDI[6]** is also compatible with existing manufacturing line that can be immediately used for batteries without further modification. These results demonstrate that both the conjugation and contortion are critical to improve rate performance of organic materials. Such design principles provide a streamlined chemical blueprint for fast charging, long lifetime, and sustainable battery electrodes.

ASSOCIATED CONTENT

Supporting Information

The Supporting Information is available free of charge on the ACS Publications website.
Synthetic details and characterization, supporting figures and tables, electrochemical data and theoretical details.

AUTHOR INFORMATION

Corresponding Author

*zj2286@columbia.edu
*yy2664@columbia.edu
*cn37@columbia.edu

Author Contributions

† Z.J and Q.C. contributed equally.

ACKNOWLEDGMENT

Primary support for this research was provided by the National Science Foundation under award DMR-2002634. The polymer synthesis was further supported by the U.S. Office of Naval Research under award N00014-20-1-2477. The Columbia University Shared Materials Characterization Laboratory was used extensively for this research. The authors acknowledge the use of instrumentation supported by NSF through the Columbia University, Materials Research Science and Engineering Center under award DMR-2011738. C.N. thanks Sheldon and Dorothea Buckler for their generous support. A.M.E. is supported by the Schmidt Science Fellows, in partnership with the Rhodes Trust. We thank Dr. Xiao Xiao and Dr. Cedric Schaack for valuable discussions.

REFERENCES

(1) Goodenough, J. B. How We Made the Li-Ion Rechargeable Battery: Progress in Portable and Ubiquitous Electronics Would Not Be Possible without Rechargeable Batteries. John B. Goodenough Recounts the History of the Lithium-Ion Rechargeable Battery. *Nat. Electron.* **2018**, *1* (3), 204.

(2) Whittingham, M. S. Lithium Batteries and Cathode Materials. *Chem. Rev.* **2004**, *104* (10), 4271–4301.

(3) Yoshino, A. The Birth of the Lithium-Ion Battery. *Angew. Chemie - Int. Ed.* **2012**, *51* (24), 5798–5800.

(4) Armand, M.; Tarascon, J.-M. Building Better Batteries. *Nature* **2008**, *451* (7179), 652–657.

(5) Manthiram, A. An Outlook on Lithium Ion Battery Technology. *ACS Cent. Sci.* **2017**, *3* (10), 1063–1069.

(6) Goodenough, J. B.; Park, K. S. The Li-Ion Rechargeable Battery: A Perspective. *J. Am. Chem. Soc.* **2013**, *135* (4), 1167–1176.

(7) Keyser, M.; Pesaran, A.; Li, Q.; Santhanagopalan, S.; Smith, K.; Wood, E.; Ahmed, S.; Bloom, I.; Dufek, E.; Shirk, M.; Meintz, A.; Kreuzer, C.; Michelbacher, C.; Burnham, A.; Stephens, T.; Francfort, J.; Carlson, B.; Zhang, J.; Vijayagopal, R.; Hardy, K.; Dias, F.; Mohanpurkar, M.; Scoffield, D.; Jansen, A. N.; Tanim, T.; Markel, A. Enabling Fast Charging – Battery Thermal Considerations. *J. Power Sources* **2017**, *367*, 228–236.

(8) Burnham, A.; Dufek, E. J.; Stephens, T.; Francfort, J.; Michelbacher, C.; Carlson, R. B.; Zhang, J.; Vijayagopal, R.; Dias, F.; Mohanpurkar, M.; Scoffield, D.; Hardy, K.; Shirk, M.; Hovsapian, R.; Ahmed, S.; Bloom, I.; Jansen, A. N.; Keyser, M.; Kreuzer, C.; Markel, A.; Meintz, A.; Pesaran, A.; Tanim, T. R. Enabling Fast Charging – Infrastructure and Economic Considerations. *J. Power Sources* **2017**, *367*, 237–249.

(9) Ahmed, S.; Bloom, I.; Jansen, A. N.; Tanim, T.; Dufek, E. J.; Pesaran, A.; Burnham, A.; Carlson, R. B.; Dias, F.; Hardy, K.; Keyser, M.; Kreuzer, C.; Markel, A.; Meintz, A.; Michelbacher, C.; Mohanpurkar, M.; Nelson, P. A.; Robertson, D. C.; Scoffield, D.; Shirk, M.; Stephens, T.; Vijayagopal, R.; Zhang, J. Enabling Fast Charging – A Battery Technology Gap Assessment. *J. Power Sources* **2017**, *367*, 250–262.

(10) Liu, Y.; Zhu, Y.; Cui, Y. Challenges and Opportunities towards Fast-Charging Battery Materials. *Nat. Energy* **2019**, *4* (7), 540–550.

(11) Augustyn, V.; Come, J.; Lowe, M. A.; Kim, J. W.; Taberna, P. L.; Tolbert, S. H.; Abruña, H. D.; Simon, P.; Dunn, B. High-Rate Electrochemical Energy Storage through Li + Intercalation Pseudocapacitance. *Nat. Mater.* **2013**, *12* (6), 518–522.

(12) Yu, Z.; Wang, H.; Kong, X.; Huang, W.; Tsao, Y.; Mackanic, D. G.; Wang, K.; Wang, X.; Huang, W.; Choudhury, S.; Zheng, Y.; Amanchukwu, C. V.;

Hung, S. T.; Ma, Y.; Lomeli, E. G.; Qin, J.; Cui, Y.; Bao, Z. Molecular Design for Electrolyte Solvents Enabling Energy-Dense and Long-Cycling Lithium Metal Batteries. *Nat. Energy* **2020**, *5* (7), 526–533.

(13) Meintz, A.; Zhang, J.; Vijayagopal, R.; Kreutzer, C.; Ahmed, S.; Bloom, I.; Burnham, A.; Carlson, R. B.; Dias, F.; Dufek, E. J.; Francfort, J.; Hardy, K.; Jansen, A. N.; Keyser, M.; Markel, A.; Michelbacher, C.; Mohanpurkar, M.; Pesaran, A.; Scoffield, D.; Shirk, M.; Stephens, T.; Tanim, T. Enabling Fast Charging – Vehicle Considerations. *J. Power Sources* **2017**, *367*, 216–227.

(14) Lu, Y.; Chen, J. Prospects of Organic Electrode Materials for Practical Lithium Batteries. *Nat. Rev. Chem.* **2020**, *4* (3), 127–142.

(15) Gannett, C. N.; Melecio-Zambrano, L.; Theibault, M. J.; Peterson, B. M.; Fors, B. P.; Abruña, H. D. Organic Electrode Materials for Fast-Rate, High-Power Battery Applications. *Mater. Reports Energy* **2021**, *1* (1), 100008.

(16) Muench, S.; Wild, A.; Friebe, C.; Häupler, B.; Janoschka, T.; Schubert, U. S. Polymer-Based Organic Batteries. *Chem. Rev.* **2016**, *116* (16), 9438–9484.

(17) Lee, S.; Kwon, G.; Ku, K.; Yoon, K.; Jung, S. K.; Lim, H. D.; Kang, K. Recent Progress in Organic Electrodes for Li and Na Rechargeable Batteries. *Adv. Mater.* **2018**, *30* (42), 1–45.

(18) Bhosale, M. E.; Chae, S.; Kim, J. M.; Choi, J. Y. Organic Small Molecules and Polymers as an Electrode Material for Rechargeable Lithium Ion Batteries. *J. Mater. Chem. A* **2018**, *6* (41), 19885–19911.

(19) Liang, Y.; Yao, Y. Positioning Organic Electrode Materials in the Battery Landscape. *Joule* **2018**, *2* (9), 1690–1706.

(20) Larcher, D.; Tarascon, J. M. Towards Greener and More Sustainable Batteries for Electrical Energy Storage. *Nat. Chem.* **2015**, *7* (1), 19–29.

(21) Hiroyuki, N.; Kenichi, O. Toward Flexible Batteries. *Science (80-.).* **2008**, *319* (5864), 737–738.

(22) Poizot, P.; Gaubicher, J.; Renault, S.; Dubois, L.; Liang, Y.; Yao, Y. Opportunities and Challenges for Organic Electrodes in Electrochemical Energy Storage. *Chem. Rev.* **2020**, *120* (14), 6490–6557.

(23) Zhong, Y.; Trinh, M. T.; Chen, R.; Wang, W.; Khlyabich, P. P.; Kumar, B.; Xu, Q.; Nam, C.-Y.; Sfeir, M. Y.; Black, C.; Steigerwald, M. L.; Loo, Y.-L.; Xiao, S.; Ng, F.; Zhu, X.-Y.; Nuckolls, C. Efficient Organic Solar Cells with Helical Perylene Diimide Electron Acceptors. *J. Am. Chem. Soc.* **2014**, *136* (43), 15215–15221.

(24) Zhong, Y.; Sisto, T. J.; Zhang, B.; Miyata, K.; Zhu, X.-Y.; Steigerwald, M. L.; Ng, F.; Nuckolls, C. Helical Nanoribbons for Ultra-Narrowband Photodetectors. *J. Am. Chem. Soc.* **2017**, *139* (16), 5644–5647.

(25) Zhong, Y.; Kumar, B.; Oh, S.; Trinh, M. T.; Wu, Y.; Elbert, K.; Li, P.; Zhu, X.; Xiao, S.; Ng, F.; Steigerwald, M. L.; Nuckolls, C. Helical Ribbons for Molecular Electronics. *J. Am. Chem. Soc.* **2014**, *136* (22), 8122–8130.

(26) Peurifoy, S. R.; Castro, E.; Liu, F.; Zhu, X.-Y.; Ng, F.; Jockusch, S.; Steigerwald, M. L.; Echegoyen, L.; Nuckolls, C.; Sisto, T. J. Three-Dimensional Graphene Nanostructures. *J. Am. Chem. Soc.* **2018**, *140* (30), 9341–9345.

(27) Castro, E.; Sisto, T. J.; Romero, E. L.; Liu, F.; Peurifoy, S. R.; Wang, J.; Zhu, X.; Nuckolls, C.; Echegoyen, L. Cove-Edge Nanoribbon Materials for Efficient Inverted Halide Perovskite Solar Cells. *Angew. Chemie Int. Ed.* **2017**, *56* (46), 14648–14652.

(28) Zhu, X.; Liu, X.; Deng, W.; Xiao, L.; Yang, H.; Cao, Y. Perylenediimide Dyes as a Cheap and Sustainable Cathode for Lithium Ion Batteries. *Mater. Lett.* **2016**, *175*, 191–194.

(29) Peurifoy, S. R.; Russell, J. C.; Sisto, T. J.; Yang, Y.; Roy, X.; Nuckolls, C. Designing Three-Dimensional Architectures for High-Performance Electron Accepting Pseudocapacitors. *J. Am. Chem. Soc.* **2018**, *140* (35), 10960–10964.

(30) Russell, J. C.; Posey, V. A.; Gray, J.; May, R.; Reed, D. A.; Zhang, H.; Marbella, L. E.; Steigerwald, M. L.; Yang, Y.; Roy, X.; Nuckolls, C.; Peurifoy, S. R. High-Performance Organic Pseudocapacitors via Molecular Contortion. *Nat. Mater.* **2021**, *20*, 1136–1141.

(31) Bhosale, M. E.; Krishnamoorthy, K. Chemically Reduced Organic Small-Molecule-Based Lithium Battery with Improved Efficiency. *Chem. Mater.* **2015**, *27* (6), 2121–2126.

(32) Zhong, Y.; Kumar, B.; Oh, S.; Trinh, M. T.; Wu, Y.; Elbert, K.; Li, P.; Zhu, X.; Xiao, S.; Ng, F.; Steigerwald, M. L.; Nuckolls, C. Helical Ribbons for Molecular Electronics. *J. Am. Chem. Soc.* **2014**, *136* (22), 8122–8130.

(33) Schuster, N. J.; Hernández Sánchez, R.; Bukharina, D.; Kotov, N. A.; Berova, N.; Ng, F.; Steigerwald, M. L.; Nuckolls, C. A Helicene Nanoribbon with Greatly Amplified Chirality. *J. Am. Chem. Soc.* **2018**, *140* (20), 6235–6239.

(34) Junqi, L.; G., B. S.; P., G. E.; Seiko, F.; J., S. M.; E., P. A. M.; W., L. J.; F., M. G.; D., B. M. Synthesis of Many Different Types of Organic Small Molecules Using One Automated Process. *Science (80-.).* **2015**, *347* (6227), 1221–1226.

(35) Blair, D. J.; Chitti, S.; Trobe, M.; Kostyra, D. M.; Haley, H. M. S.; Hansen, R. L.; Ballmer, S. G.; Woods, T. J.; Wang, W.; Mubayi, V.; Schmidt, M. J.; Pipal, R. W.; Morehouse, G. F.; Palazzolo Ray, A. M. E.; Gray, D. L.; Gill, A. L.; Burke, M. D. Automated Iterative Csp3–C Bond Formation. *Nature* **2022**, *604* (7904), 92–97.

(36) Schuster, N. J.; Hernández Sánchez, R.; Bukharina, D.; Kotov, N. A.; Berova, N.; Ng, F.; Steigerwald, M. L.; Nuckolls, C. A Helicene Nanoribbon with Greatly Amplified Chirality. *J. Am. Chem. Soc.* **2018**, *140* (20), 6235–6239.

(37) Wu, J.; Rui, X.; Long, G.; Chen, W.; Yan, Q.;

Zhang, Q. Pushing Up Lithium Storage through Nanostructured Polyazaacene Analogues as Anode. *Angew. Chemie - Int. Ed.* **2015**, *54* (25), 7354–7358.

(38) Meier, H.; Stalmach, U.; Kolshorn, H. Effective Conjugation Length and UV/Vis Spectra of Oligomers. *Acta Polym.* **1997**, *48* (9), 379–384.

(39) Liang, Y.; Chen, Z.; Jing, Y.; Rong, Y.; Facchetti, A.; Yao, Y. Heavily N-Dopable π-Conjugated Redox Polymers with Ultrafast Energy Storage Capability. *J. Am. Chem. Soc.* **2015**, *137* (15), 4956–4959.

(40) Wang, S.; Wang, Q.; Shao, P.; Han, Y.; Gao, X.; Ma, L.; Yuan, S.; Ma, X.; Zhou, J.; Feng, X.; Wang, B. Exfoliation of Covalent Organic Frameworks into Few-Layer Redox-Active Nanosheets as Cathode Materials for Lithium-Ion Batteries. *J. Am. Chem. Soc.* **2017**, *139* (12), 4258–4261.

(41) Ho, C.; Raistrick, I. D.; Huggins, R. A. Application of A-C Techniques to the Study of Lithium Diffusion in Tungsten Trioxide Thin Films. *J. Electrochem. Soc.* **1980**, *127* (2), 343–350.

(42) Gannett, C. N.; Peterson, B. M.; Shen, L.; Seok, J.; Fors, B. P.; Abruña, H. D. Cross-Linking Effects on Performance Metrics of Phenazine-Based Polymer Cathodes. *ChemSusChem* **2020**, *13* (9), 2428–2435.

Insert Table of Contents artwork here